View metadata, citation and similar papers at core.ac.uk

brought to you by CORE

provided by Nottingham Trent Institutional Repository (IRep)

Journal Pre-proofs

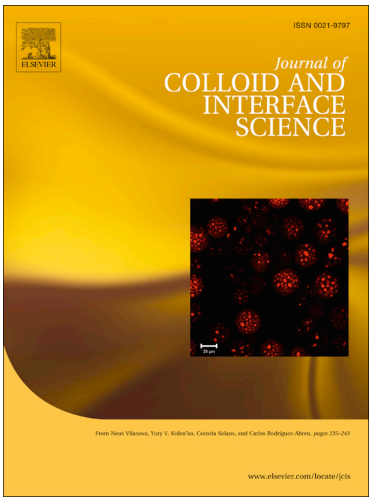

Enhancement of cadmium removal by oxygen-doped carbon nitride with molybdenum and sulphur hybridization

Jing Su, Lei Bi, Chen Wang, Tao Lyu, Gang Pan

PII: S0021-9797(19)31013-6
DOI: https://doi.org/10.1016/j.jcis.2019.08.104
Reference: YJCIS 25360

To appear in: *Journal of Colloid and Interface Science*

Received Date: 16 June 2019
Revised Date: 26 August 2019
Accepted Date: 27 August 2019

Please cite this article as: J. Su, L. Bi, C. Wang, T. Lyu, G. Pan, Enhancement of cadmium removal by oxygen-doped carbon nitride with molybdenum and sulphur hybridization, *Journal of Colloid and Interface Science* (2019), doi: https://doi.org/10.1016/j.jcis.2019.08.104

This is a PDF file of an article that has undergone enhancements after acceptance, such as the addition of a cover page and metadata, and formatting for readability, but it is not yet the definitive version of record. This version will undergo additional copyediting, typesetting and review before it is published in its final form, but we are providing this version to give early visibility of the article. Please note that, during the production process, errors may be discovered which could affect the content, and all legal disclaimers that apply to the journal pertain.

© 2019 Published by Elsevier Inc.

Journal Pre-proofs

Enhancement of cadmium removal by oxygen-doped carbon nitride with molybdenum and sulphur hybridization

Jing Su [a,d], Lei Bi *[a], Chen Wang [a,d,e], Tao Lyu [b,c], Gang Pan *[a,b,c,d,e]

[a] *Key Laboratory of Environmental Nanotechnology and Health Effects, Research Center for Eco-Environmental Sciences, Chinese Academy of Sciences, Beijing 100085, P. R. China*

[b] *School of Animal, Rural, and Environmental Sciences, Nottingham Trent University, Brackenhurst Campus, NG25 0QF, UK*

[c] *Centre of Integrated Water-Energy-Food studies (iWEF), Nottingham Trent University, Nottinghamshire, NG25 0QF, UK*

[d] *University of Chinese Academy of Sciences, Beijing 100049, P. R. China*

[e] *Sino-Danish College of University of Chinese Academy of Sciences, Beijing 100049, P. R. China*

Authors: Jing Su, e-mail: sujingwendy@hotmail.com

Chen Wang, e-mail: catherineb612@foxmail.com

Tao Lyu, e-mail: tao.lyu@ntu.ac.uk

Corresponding authors: * Gang Pan, Phone: +86-10-62849686; e-mail: gpan@rcees.ac.cn (G. Pan)

* Lei Bi, Phone: +86-10-62943436; e-mail: leibi@rcees.ac.cn (L. Bi)

Declaration of interest: none.

Journal Pre-proofs

Journal Pre-proofs

Abstract

Graphitic carbon nitride, as a popular material in the field of environmental remediation, still suffers from unsatisfactory performance for heavy metals adsorption owing to lack of specific adsorption sites. In this study, molybdenum (Mo) and sulphur (S) were simultaneously introduced onto the surface of oxygen-doped graphitic carbon nitride (OCN) for the enhancement of Cd^{2+} adsorption. The synthesized MOS/OCN-1 exhibited substantially increased maximum adsorption capacity of 293.8 mg/g, calculated from Sips isotherm model, which was 8.7 times higher than that for pristine OCN (33.9 mg/g). The adsorption efficiency of MOS/OCN-1 was >94% even under high concentration of coexisting ions (ie. Ca^{2+}, Mg^{2+} and Zn^{2+}). MoO_3 and MoS_2 on the surface of OCN were proven to interact with Cd^{2+} by forming $CdMoO_4$ and CdS species. OCN provided a stable matrix with a large surface area making more active sites exposed, which greatly facilitated Mo(IV) oxidation and Cd^{2+} precipitation. Our findings revealed that as well as the well-known Cd-S interaction, Mo atoms in the hybrid composites also played an important role in Cd^{2+} removal, which opened up the application possibility of OCN with Mo and S hybridization for *in-situ* Cd^{2+} remediation.

Keywords: Cadmium adsorption; graphitic carbon nitride; heavy metals removal; molybdenum compound; nano material

1. Introduction

Over the past decades, cadmium (Cd^{2+}) contamination of farmland and natural waters has been of increasing concern due to its high toxicity and persistence [1, 2]. In some cases, contamination has led to deleterious effects on the human health, including reproductive disorder,

Journal Pre-proofs

liver damage or carcinogenicity, when cadmium, even at trace concentrations, entered into human bodies through the food web [1, 3-6]. Adsorption has long been considered as a promising method for the remediation of Cd^{2+} polluted soils and waters due to its characteristics of low cost, high efficiency and simple operation when compared with other techniques such as flocculation, membrane filtration, biological remediation and electrochemical treatment [2, 7]. Hence, in order to ensure food and drinking water safety, the exploration of efficient adsorbents for Cd^{2+} removal is an urgent need.

Graphitic carbon nitride (g-C_3N_4) is a carbon based material with graphene-like structure, which has attracted much attention for the degradation of organic pollutants due to its semiconductor properties, long-term stability and environmental friendliness [8]. Several studies have also proven the efficacy of bulk g-C_3N_4 for the removal of heavy metals, e.g. Cd(II), Pb(II), Cu(II), Ni(II) and Cr(VI), but only modest adsorption capacities have been achieved [6, 9, 10], since the relative less active sites of bulk g-C_3N_4 hinder the achievement of higher adsorption efficiency [11]. In order to improve the adsorption ability towards heavy metals, several studies attempted to introduce new active sites onto the bulk g-C_3N_4. Zou et al [12] modified β-cyclodextrin on g-C_3N_4 and the synthesized compounds exhibited a significantly improved adsorption capacity towards Pb^{2+} due to the induced oxygen-containing groups. Wang et al [13] decorated g-C_3N_4 with polyethyleneimine in order to increase the number of functional groups (C-C, C-O, N-C=C, etc), and the modified material performed superior complexation of U(VI) and Am-243(III). Moreover, enlarging the surface area of the adsorbent may further enhance the adsorption capacity by providing additional adsorption sites. Qiu et al [14] reported that the oxygen-doping of graphic carbon nitride (OCN) could substantially increase the surface area of g-C_3N_4 and facilitate the

adsorption of organic pollutants. However, OCN hasn't yet been tested for the adsorption of heavy metals. We hypothesize that modification of OCN by inclusion of active groups might overcome the challenges of limited adsorption active sites and surface area, enabling more effective Cd^{2+} removal.

It is well known that S^{2-}/-HS are effective groups for the capture of heavy metals due to strong soft-soft interactions with heavy metals according to Pearson's theory [15, 16]. MoS_2, as one of the typical molybdenum compounds with a large amount of intrinsic sulphur, has been proven to be a promising adsorbent for the removal of Hg^{2+} [17, 18], Pb^{2+} [19], and Cd^{2+} [20]. Intensive studies have shown that disulphide (S-S) planes in MoS_2 are active, and that S^{2-} can act as soft base to form M-S complex with Hg/Pb/Cd soft acid through electron interaction and covalent bonding [17, 18, 20]. As a comparison, the direct effects and mechanisms of Mo atoms on Cd^{2+} adsorption are rarely investigated. Several studies demonstrated that MoS_2 is thermodynamically unstable in the aerobic and high moisture conditions, where Mo(IV) is likely to be oxidized to Mo(VI), such as MoO_3 [21, 22]. The oxidized Mo(VI) has been demonstrated to be able to immobilize Pb^{2+}/Hg^{2+} by forming $PbMoO_4$ or a Mo-O-Hg complex [23, 24]. Since the similar soft-acidic property of Cd^{2+} is shared by Hg^{2+} and Pb^{2+}, different valencies of Mo may also influence the adsorption behaviour for Cd^{2+}. Thus, these mechanisms, particularly the possibly synergistic effects of Mo and S, for improving Cd^{2+} removal are in need of investigation.

In this study, we prepared oxygen-doped graphitic carbon nitride (OCN) and then simultaneously introduced Mo and S on the surface via a facile hydrothermal method, to produce the hybrid adsorbent (MOS/OCN) which was considered suitable for Cd^{2+} removal. In order to evaluate the enhanced Cd^{2+} adsorption performance, MOS/OCN was optimized and the adsorption capacity was compared to pristine OCN, MoS_2 and other published adsorbents. The adsorption

Journal Pre-proofs

kinetics and isotherm were evaluated to address the adsorption behaviours of Cd^{2+}. The anti-interference ability of MOS/OCN was also investigated under the coexistence of competitive ions, i.e. Ca^{2+}, Mg^{2+} and Zn^{2+}, during Cd^{2+} removal. Lastly, in order to elucidate the adsorption mechanisms of Cd^{2+}, the effects of Mo (IV /VI) and S atoms on the Cd^{2+} adsorption process were further assessed. With these results, this study aims to suggest a new effective adsorbent for Cd^{2+} removal with an explanation of fundamental mechanisms involved.

2. Materials and Methods

2.1 Reagents

Urea (>99%), oxalic acid dehydrate (≥99.5%), ammonium molybdate tetrahydrate ($(NH_4)_6 Mo_7O_{24}{\cdot}4H_2O$, >99%), thiourea (> 99%) and metal nitrate (Cd(II), Zn(II), Mg(II), Ca(II), > 99%) were purchased from Sinopharm Chemical Regent Co. Ltd. N, N-Dimethylformamide (DMF, > 99.8%) was obtained from J&K Chemical Reagent Co., Ltd. Deionized water was used in all experiments.

2.2 Synthesis of Adsorbents

2.2.1 Synthesis of oxygen-doped graphitic carbon nitride (OCN)

The OCN was synthesized according to Qiu et al, 2017 [14] with slight modification. Briefly, urea (10 g) and oxalic acid dehydrate (4 g) were mixed by grinding in a mortar. The mixture powder was then transferred into a quartz boat and calcined at 550°C for 4 h with a heating rate of 3°C/min in an atmosphere of N_2.

2.2.2 Synthesis of MOS/OCN-x hybrid composites

Firstly, OCN (80 mg) was added into pre-mixed solution composed of DMF (64 mL) and deionized water (16 mL) and sonicated for 1 h to form a homogeneous solution. Then, a required amount of $(NH_4)_6Mo_7O_{24}\cdot 4H_2O$ and thiourea were added into this mixed solution and stirred at

Journal Pre-proofs

60°C for 30 min to ensure those reagents were totally dissolved. The molar ratio of $(NH_4)_6Mo_7O_{24} \cdot 4H_2O$ and thiourea was kept in constant of 1:30. The mixture was further sonicated for 1h and then transferred into 100 mL Teflon stainless steel autoclave and heated to 180°C for 18 h. After cooling down to ambient temperature, the solid samples were collected by centrifugation and washed sequentially three times with deionized water and absolute ethyl alcohol. Finally, the solid was dried at 60°C for 12 h in the vacuum oven. The ultimate sample was denoted as MOS/OCN-x, where x equalled to 0.5, 1, 2 and 4 when the mass ratio of $(NH_4)_6Mo_7O_{24} \cdot 4H_2O$ to OCN was 0.5:1, 1:1, 2:1 and 4:1, respectively. Molybdenum disulphide, named as MOS-DMF, was also prepared by this procedure but without addition of OCN.

2.2.3 Synthesis of MoO_3/OCN

The pure MoO_3 was prepared via a facile hydrothermal reaction, according to Liu et al., 2016 [25]. Then, a required amount of MoO_3 powder, of which the total Mo was equal to that of MOS/OCN-1 was ground with OCN (80 mg) by mortar and pestle for 30 min and added into solution composed of DMF (64 mL) and H_2O (16 mL) for further sonication treatment (1 h). The mixed solution was transferred into 100 mL Teflon-lined autoclave and heated to 180°C for 18 h. The synthesized MoO_3/OCN solid was then collected and dried under vacuum at 60°C.

2.3 Adsorption experiments

In order to determine the optimal composition of MOS/OCN, the Cd^{2+} adsorption capabilities by MOS/OCN-x (x=0.5, 1, 2, 4), MOS-DMF, and OCN were evaluated. In the adsorption experiment, adsorbent (5 mg) was added into Cd^{2+} solution (20 mL) with an initial concentration of 20 mg/L. The mixture was then agitated at 130 rpm for 24 h under 25°C. The solution pH was kept at 6.0 ± 0.2 by adding 0.1 M HNO_3 or 0.1 M NaOH. After the reaction, 3 mL supernatant was collected and filtered

Journal Pre-proofs

129 through 0.22 µm pore size membrane for determination of Cd^{2+} concentration.

130 The optimal MOS/OCN-1 was further utilised in the Cd^{2+} removal kinetics and isotherm
131 experiments in order to evaluate adsorption behaviours. For the kinetics experiment, dosages of
132 0.25 g/L MOS/OCN-1, MOS-DMF, and OCN were separately added to Cd^{2+} solution (20 mg/L, 20 mL)
133 at constant pH (6.0 ± 0.2) and temperature (25°C). During the experiment, the suspensions were
134 collected from 0-36 h to determine the Cd^{2+} concentration. Pseudo-first order, pseudo-second order
135 and intraparticle diffusion models were used to simulate experimental data (Supporting Information,
136 S1). The adsorption isotherm study was further performed to determine the maximum Cd^{2+}
137 adsorption capacity. Briefly, MOS/OCN-1, MOS-DMF, and OCN (each 5 mg) were separately added
138 into Cd^{2+} solution (20 mL) with initial concentrations of 15-600 mg/L at pH 6.0 ± 0.2 and 25 °C. After
139 24 h, the supernatant was taken for analysis of Cd^{2+} concentration. Langmuir, Freundlich and Sips
140 isotherm models were conducted to simulate the experimental data (Supporting Information, S1).
141 The Cd^{2+} removal efficiency and the adsorption capacity were calculated as followings:

142 $$\eta = \frac{(C_0 - C_e)}{C_0} \times 100\% \quad (1)$$

143 $$q_e = \frac{(C_0 - C_e) \times V}{m} \quad (2)$$

144 Where η (%) is Cd^{2+} removal efficiency, C_0 and C_e are the initial and equilibrium concentration of Cd^{2+} in
145 solution (mg/L), respectively. q_e (mg/g) is Cd^{2+} adsorption capacity in equilibrium state, V is the volume of
146 Cd^{2+} solution and m is the mass of adsorbents.

147 In order to evaluate the effect of pH on the Cd^{2+} adsorption by the optimal adsorbent
148 MOS/OCN-1, the adsorption capacity was determined under different pH values of 2, 3, 4, 5, and 6
149 with an initial Cd^{2+} of 20 mg/L. In addition, the effect of competing cations on Cd^{2+} adsorption was

also evaluated. During the adsorption experiment, the ions Ca^{2+}, Mg^{2+}, and Zn^{2+}, at concentrations of 0, 10, 50, and 100 mg/L were added separately into the Cd^{2+} solutions (10 mg/L) and the finial Cd^{2+} was analyzed. To further confirm the selectivity and anti-interference ability of MOS/OCN-1 towards Cd^{2+}, the mixed solution contained Cd^{2+}, Ca^{2+}, Mg^{2+} and Zn^{2+} in which each cation ion was 10 mg/L, was treated by MOS/OCN-1 (0.25 g/L) followed the same procedure of the adsorption experiment. The remnant cation ions were determined after 24 h for the further removal efficiency and distribution coefficient calculation. The distribution coefficient K_d (mL/g), a measurement of affinity and selectivity [26] for each cation ions was calculated according to Equation (3):

$$K_d = \frac{V(C_0 - C_f)}{m \quad C_f} \tag{3}$$

Where C_0 and C_f (mg/L) represent the initial and equilibrium concentrations of the ions, V is the solution volume (mL) and m (mg) is the mass of adsorbent.

To investigate the reusability of the adsorbent, the Cd^{2+} loaded MOS/OCN-1 was used for the Cd^{2+} desorption and re-adsorption experiments. To initiate the desorption process, HNO_3 (250 mL, 0.1M) were added to the residue adsorbent solid (62.5 mg) and mixture was then shaken at 130 rpm at 25°C for 2h. At the end of the desorption test, the residue MOS/OCN-1 was collected and dried at 60 ℃ for 24 h for the further re-adsorption study. The re-adsorption test was performed in 50 mL centrifuge tubes contained MOS/OCN-1 (0.25g/L) and Cd^{2+} solution (10 mg/L) with pH kept at 6. The Cd^{2+} concentration was determined after each adsorption-desorption cycle.

To further discover how different valencies of Mo atoms may affect Cd^{2+} adsorption, the removal efficiency of Cd^{2+} by MoO_3/OCN was compared with MOS/OCN-1. The adsorbent dosage, initial Cd^{2+} solution and environmental conditions were the same as previously described. All the aforementioned adsorption experiments were conducted in duplicate and each sample analysis was

Journal Pre-proofs

conducted in triplicate.

2.4 Sample analysis

2.4.1 Water samples analysis

All water samples were filled through a 0.22 μm cellulose acetate membrane and acidized by 1% HNO_3 before analysis. The concentration of Cd^{2+}, the leached MoO_4^{2-} and dissolved total S in the filtrate was determined by inductively coupled plasma-optical emission spectrometer (ICP-OES; Optima 8300, Perkin Elmer Inc., USA) with a detection limit of 0.2 mg/L. It should be noted that the inductively coupled plasma-mass spectroscopy (ICP-MS; 7500a, Agilent Inc. USA) was used to confirm the results when the concentration level below 0.2 mg/L.

2.4.2 Adsorbents characterization

The adsorbent structure and crystal phase were recorded by X-ray diffraction (XRD) patterns using a PANalytical X'Pert PRO powder diffraction system (Malvern Panalytical, Cambridge, UK) with Cu K_α radiation (λ=1.5418Å) and scanning speed of 5°/min from 5°-90°/2θ. The morphology of adsorbents was examined by field emission scanning electron microscopy (FESEM; Su-8020, Hitachi, Japan) with an acceleration voltage of 35 kV. X-ray photoelectron spectroscopy data (XPS; SCALAB250Xi, Thermo Fisher Scientific, USA) was collected with a monochromatic Al K_α radiation source (1486.6 eV). The specific surface areas of the original synthesized adsorbents were detected according to the Brunauer-Emmett-Teller (BET) method (Micromeritics ASAP 2020 Analyzer, Mack instruments, Inc., USA). Before BET measurement, the samples were degassed at 80°C for 6 h. Moreover, the characteristics of the surface functional groups presented on the adsorbents were investigated on a Fourier transform infrared spectra (FTIR; Nicolet 8700, Thermo Fisher Scientific, USA) with the wavenumber of 4000-400 cm^{-1}.

Journal Pre-proofs

3. Results and discussion

3.1 Characterization and optimization of adsorbents

After synthesis, the XRD patterns of MOS/OCN-x, MOS-DMF, and OCN were analyzed (Fig. 1a). The original OCN exhibited clear diffraction peak at 2θ= 27.2° ascribed to the (002) plane of g-C_3N_4 [14]. The peak intensity decreased along with the increased mass of Mo and S hybridization (increased x value) for MOS/OCN-x, which was attributed to relatively low content of OCN. For MOS-DMF, the two peaks at 9.34° and 18.44° represented (001) and (002) plane of MoS_2 , which were split from the pristine (002) plane of 14.13°, suggesting that the new lamellar structure had been formed due to relatively low hydrothermal temperature at 180°C [27, 28]. Two other peaks at 32.87° and 57.71° can be indexed to the (100) and (110) planes of MoS_2 (JCPDS card No. 075-1539), respectively. Therefore, MoS_2 was confirmed to be the main composition of MOS-DMF. Besides characteristic peaks of MoS_2, peaks attributable to the (310) and (430) planes of MoO_3 (JCPDS card no. 21-0569) emerged in the hybrid composite of MOS/OCN-x and became more obvious when x decreased to 0.5 or 1, which probably because the moderate content of OCN presented in that material and facilitated the transformation of MoS_2 to MoO_3 during synthesis process. Therefore, it is suggested that both MoS_2 and MoO_3 coexisted on the OCN surface in compounds MOS/OCN-x, especially when $x < 2$, while MOS-DMF mainly comprised MoS_2.

OCN exhibited much higher BET surface area (74.4 m^2/g) than MOS-DMF (24.7 m^2/g). Corresponding with the increasing incorporation of Mo and S onto OCN, the surface areas of these adsorbents significantly decreased from 74.8 m^2/g for MOS/OCN-0.5 to 21.8 m^2/g for MOS/OCN-4 (Table S1). Conventionally, a large specific surface area of an adsorbent could potentiate the removal abilities by providing more reaction sites [29]. In this study, this was supported by the

Journal Pre-proofs

results that the adsorption capacity decreased from 68.0 mg/g for MOS/OCN-1 to 24.3 mg/g for MOS-DMF with commensurate decreases in BET surface area (Fig.1b). However, OCN and MOS/OCN-0.5 showed unsatisfactory adsorption performances although both of them exhibited high specific surface areas. The limited adsorption capacities of OCN and MOS/OCN-0.5 probably resulted from the lack of sufficient active species, such as Mo and S. Thus, the synergistic effects of both the specific surface area and the number of active sites contributed to effective Cd^{2+} removal. By control of the hybridization amount of Mo and S on the surface of OCN, the synthesized adsorbent MOS/OCN-1 possessed the largest Cd^{2+} adsorption capacity and was thus selected as the optimum adsorbent.

Differing morphologies of MOS-DMF and MOS/OCN-1 were also observed. The FESEM images of MoS_2-DMF showed MoS_2 nanoparticles stacked layer by layer, exhibiting severe agglomeration (Fig.S1a). However, for MOS/OCN-1, the edge of the hybrid composite became wrinkled and several nanosheets of MoS_2 and MoO_3 erected separately (Fig. S1b), which indicated that OCN might effectively retard the agglomeration of active particles, thus possibly leading to the exposure of more suitable active sites and further enhancement of Cd^{2+} removal.

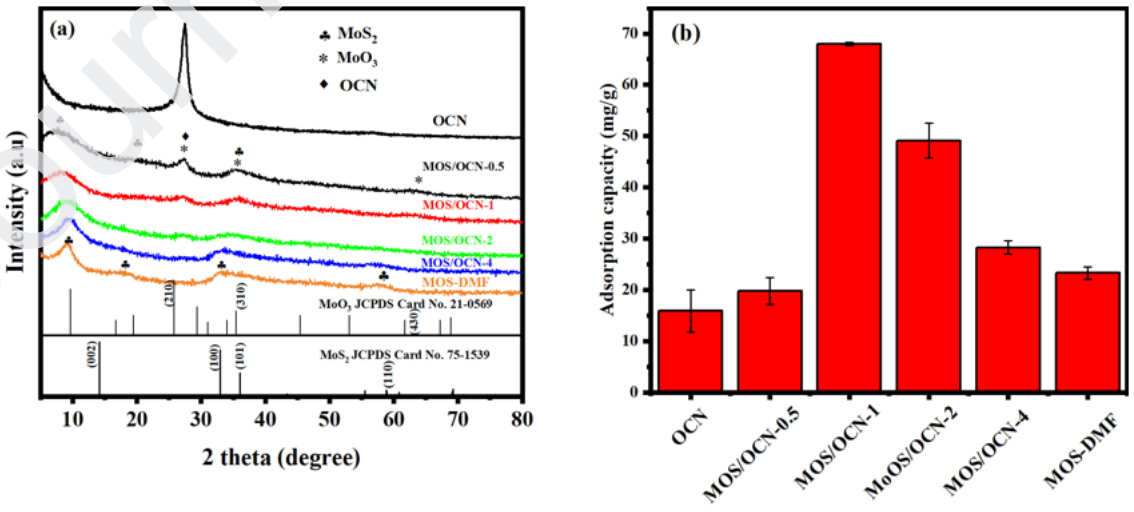

Journal Pre-proofs

Fig. 1. (a) XRD patterns of synthesized adsorbents of MOS/OCN-x, MOS-DMF, and OCN; (b) Cd^{2+} adsorption capacities of MOS/OCN-x, MOS-DMF and OCN. Experimental conditions: adsorbents dosage=0.25 g/L, initial Cd^{2+}= 20 mg/L, pH=6.0, reaction time=24 h, temperature=25°C.

XPS spectra was collected to further investigate the surface properties of the synthesized adsorbents (Fig. 2 and Table S2). MOS/OCN-1 was used to illustrate the typical spectra acquired from analyses of MOS/OCN-x. The peak at 286.4 eV in C1s of MOS/OCN-1 (Fig.S2a) could be assigned to C-O groups [30], which resulted from partial substitution of O atoms for N atoms in g-C_3N_4 [14]. In comparison, the C-O peak can be neglected in MOS-DMF due to lack of OCN in that material. The peak of Mo-C (284.2 eV) or Mo-N (394.8 eV) [31] cannot be found in MOS/OCN-1. However, when compared to pure OCN and physical mixed MoS_2+OCN, the slightly shift of N-C=N and C-N-H groups to lower binding energies accompanied with negative shift of Mo 3p occurred in MOS/OCN-1 (Fig. S2b-c). The results suggest that hydrogen bonding between OCN and Mo, S species rather than a strong chemical interaction, probably existed in the heterogenous interface. Typical peaks due to both Mo(IV) (229.0 eV and 232.84 eV) from MoS_2 and Mo(VI) (229.7 eV and 235.84 eV) from MoO_3 [25, 32, 33] were found in MOS/OCN-1 (Fig. 2a), which confirmed the coexistence of MoS_2 and MoO_3. MoO_3 was likely formed by oxidization of MoS_2 on the surface of oxygen-rich OCN after Mo and S hybridization, a hypothesis supported by the clearly larger peak area of MoO_3 (530.9 eV) [18] in Fig.2c. As a result of MoS_2 oxidization, the peak at 168.6 eV corresponding to SO_3^{2-} [34] was also observed in MOS/OCN-1 (Fig. 2b). Compared with MOS/OCN-1, much lower intensity of SO_3^{2-} and MoO_3 peaks were observed in MOS-DMF when OCN was not included during the synthesis of adsorbent (Fig. 2e-f). Moreover, Mo(VI) content in the absorbents (Table S2) showed a positive correlation with Cd^{2+} adsorption capacity (Fig. 1b). Previous studies have demonstrated that Mo(VI)

Journal Pre-proofs

254 also positively influenced the immobilization of other heavy metals, such as Pb^{2+} and Hg^{2+} [23, 24].
255 Hence, Mo atoms and the oxidization phenomenon may be key factors in influencing Cd^{2+}
256 adsorption.

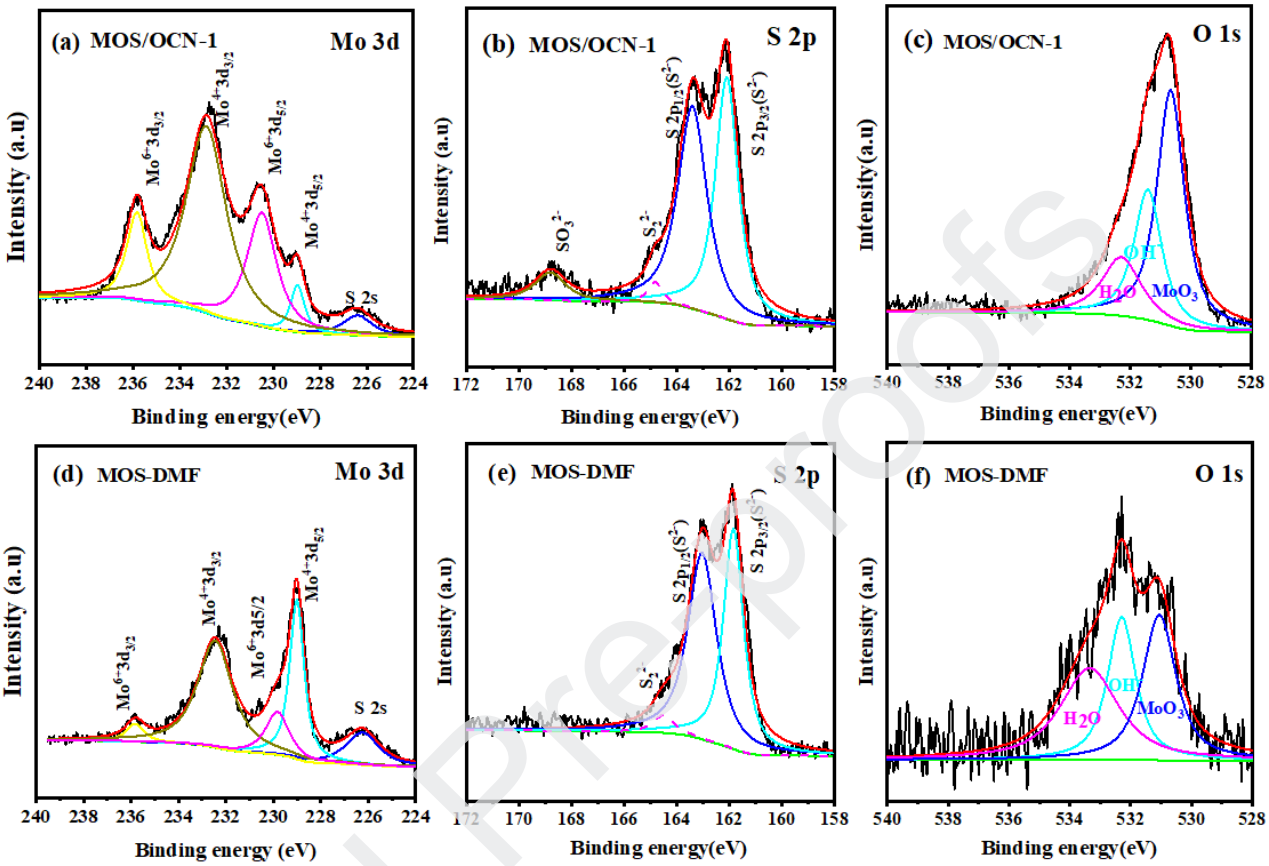

257

258 **Fig. 2**. XPS spectra of MOS/OCN-1: Mo 3d (a), S 2p (b) and O 1s (c). MOS-DMF: Mo 3d (d), S 2p (e) and O 1s
259 (f).

260 **3.2 Adsorption kinetics and isotherms**

261 MOS/OCN-1, as the optimum Cd^{2+} adsorbent, was selected to conduct Cd^{2+} adsorption kinetics
262 study and the results were compared with those using OCN and MOS-DMF (Fig. 3a). All three
263 adsorbents shown rapid adsorption rate during the initial stage within 10 mins but all subsequently
264 slowed down until an equilibrium was reached by 24 h. Pseudo-first order model and pseudo-
265 second order model were initially applied to simulate the kinetic data (Fig.3a and Fig.S3) and the

Journal Pre-proofs

related parameters were listed in Table S3. The adsorption processes of all three adsorbents were better fitted to the pseudo-second order model (R^2>0.99), which supported the premise that adsorption process was dominated by chemisorption [35]. It is clear that MOS/OCN-1 performed the highest capacity of 62.5 mg/g, followed by MOS-DMF (22.7 mg/g) and OCN (11.45 mg/g).

The results from an intraparticle diffusion model simulation (Fig. 3b) indicated that, besides chemisorption, diffusion processes, especially intraparticle diffusion, may also affect the Cd^{2+} adsorption rate on a solid solution interface. Data from all three adsorbents could be fitted into a multi-linear plot (Fig. 3b) where the first, second and third plot portions could be ascribed to bulk diffusion, intraparticle diffusion and final equilibrium, respectively [20, 36]. The slope of second plot was lower than that of the initial stage, indicating that intraparticle diffusion had slowed down, probably due to lower Cd^{2+} concentration after rapid boundary layer diffusion [36]. The k_{i2} value of MOS/OCN-1 (0.32 mg/ g·$min^{1/2}$) was higher than that of MOS-DMF (0.29 mg/g·$min^{1/2}$) and OCN (0.07 mg/g·$min^{1/2}$), which can be explained by the greater dispersion of MoS_2 and MoO_3 nanosheets on the surface of OCN in MOS/OCN-1, thus inducing more favourable contact of Cd^{2+} with interlayer active sites. It should be noted that both the first and second linear segments (Fig. 3b) did not pass through the origin, indicating that intraparticle diffusion was not the only rate-controlling step [20, 36] and that both surface chemical interaction and boundary layer control could have also potentially affected the adsorption process.

The equilibrium adsorption capacity initially increased rapidly and then gradually reached saturation with increasing equilibrium concentration of Cd^{2+} (Fig. 3c). Langmuir, Freundlich and Sips isotherm models (Supplementary Information S1) were applied to fit the equilibrium adsorption data in order to further investigate Cd^{2+} adsorption behaviour. It was obvious that the Sips isotherm

Journal Pre-proofs

model possessed the best overall fit of the experimental data ($R^2 \geq 0.95$) for MOS/OCN-1, MOS-DMF and OCN (Table S4). Since the Sips model is a combination of the Langmuir and Freundlich models, the best fitting result with 1/n not close to unity indicated that the surfaces of the three adsorbents were heterogenous [37]. For MOS-DMF and MOS/OCN-1, the heterogeneous surface probably derived from multiple sites (Mo and S) active towards Cd^{2+}, while for OCN the heterogenous surface might originate from pores resulting from overlapping layers [20]. By calculating the maximum adsorption capacity according to the Sips isotherm equation, MOS/OCN-1 exhibited the highest maximum adsorption capacity of 293.8 mg/g, which was 2.1 times and 8.7 times higher than MOS-DMF and OCN, respectively. Additionally, MOS/OCN-1 showed better Cd^{2+} adsorption performance when comparing with the adsorption capacity (9.9-205 mg/g) of other carbon-based materials or hybridized composites (Table 1). By considering the relatively low cost of MOS/OCN-1 (4,970 $/kg Cd removal) compared with other materials (4,159-35,261 $/kg Cd removal) (Table S5), it can be concluded that MOS/OCN-1 can act as a low-cost and high-efficiency adsorbent for Cd^{2+} remediation.

Journal Pre-proofs

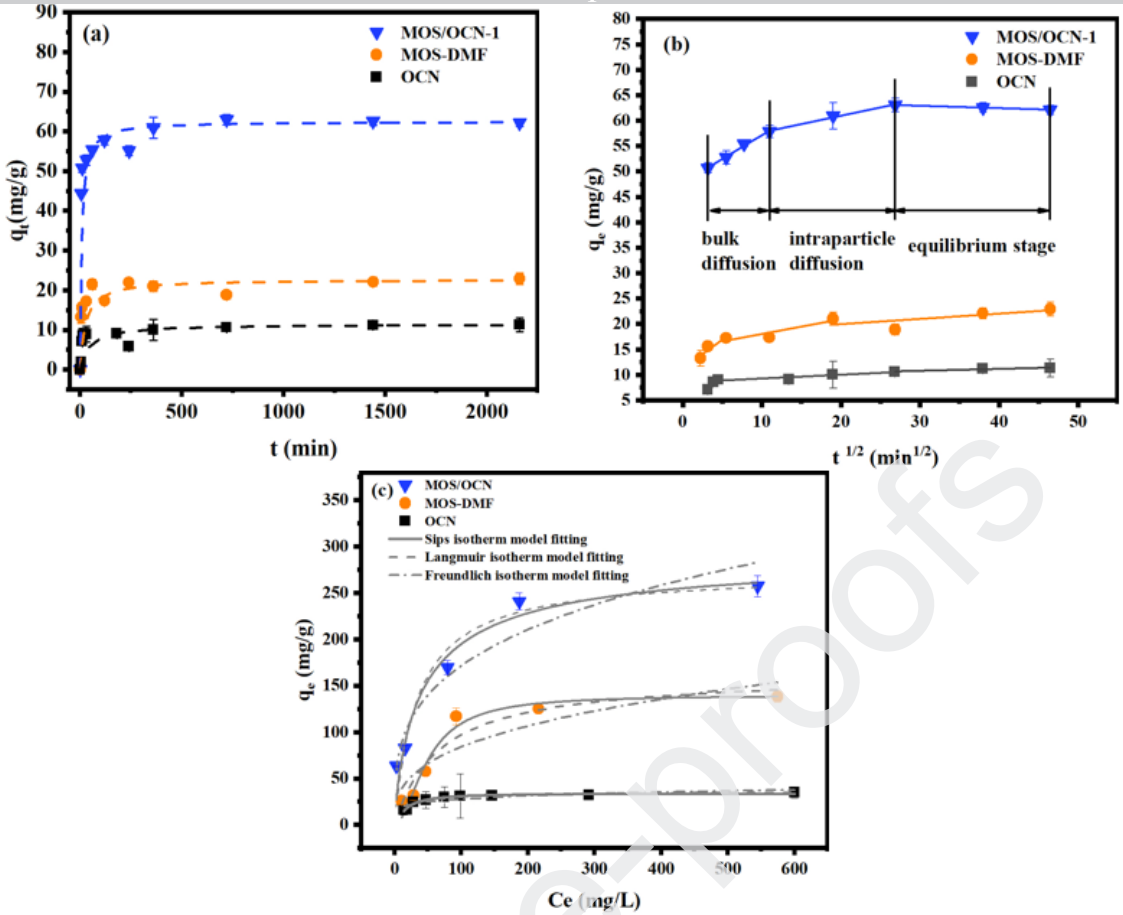

302

303 **Fig. 3**. Cd^{2+} adsorption kinetics fitted with the pseudo-second order model (a) and intraparticle diffusion

304 model (b). Experimental condition: adsorbents dosage= 0.25 g/L, initial Cd^{2+}=20 mg/L, pH=6.0 ± 0.2,

305 temperature=25°C. Cd^{2+} adsorption isotherm curve fitted with Langmuir, Freundlich and Sips model (c).

306 Experimental conditions: adsorbents dosage=0.25 g/L, initial Cd^{2+}=15-600 mg/L, pH=6.0 ± 0.2, reaction

307 time=24h, temperature=25°C.

308 **Table 1**

309 Comparison of maximum Cd^{2+} adsorption capacities by different adsorbents.

Adsorbent	q_m (mg/g)	Reference
g-C_3N_4	112.4	[9]
2D –g-C_3N_4	94.4	[6]
B-doped g-C_3N_4	159.2	[38]
Fe_3O_4-g-C_3N_4	204.5	[39]
Disulfide linked polymer networks (COP 63)	9.9	[40]

Journal Pre-proofs

TCB-700 (biologically modified biochar)	173.4	[41]
OCN	33.9	This work
MOS-DMF	139.4	This work
MOS/OCN-1	293.8	This work

3.3 Influences of pH and competing ions on Cd^{2+} adsorption

Cd^{2+} contaminated water is always found to exist under the acid condition with pH value ranges from 2-6 [42-45]. To further evaluate the effect of pH on Cd^{2+} adsorption by MOS/OCN-1, the adsorption capacity was determined separately under these conditions (Fig. 4a). The result suggested that Cd^{2+} adsorption by MOS/OCN-1 improved with increasing pH. In strong acid conditions, such as pH of 2 or 3, the uptake amount of Cd^{2+} by MOS/OCN-1 (<10 mg/g) was much lower than that at pH 6 (63 mg/g), which may be ascribed to strong electrostatic repulsion between the surface of the adsorbent and Cd^{2+} when large amounts of H^+ were present in solution [20]. The inhibiting effect of H^+ reduced under the increased pH condition, thus Cd^{2+} could approach easily to the surface of the adsorbent for further reaction.

Ca^{2+} and Mg^{2+}, as common ions in natural and wastewater, may have adverse effects on Cd^{2+} adsorption due to competition in occupying the active sites in adsorbents [46]. Moreover, Zn^{2+} has a similar hydrated ion radius (4.30 Å) to Cd^{2+} (4.26 Å) which may also inhibit Cd^{2+} adsorption [47]. Therefore, competition adsorption experiments, with different mass ratios of Ca^{2+}, Mg^{2+}, Zn^{2+} to Cd^{2+} (1:1, 5:1, 10:1) were performed in order to determine their effects on Cd^{2+} adsorption. The result in Fig. 4b illustrated that the adsorption efficiency of Cd^{2+} still remained 98.5% when both Ca^{2+} and Mg^{2+} concentrations were up to 100 mg/L. The presence of Zn^{2+} at a concentration of 100 mg/L only produced a slight decreased efficiency from 99.2% to 94.6%. Thus, the three coexisting ions, Ca^{2+}, Mg^{2+}, and Zn^{2+}, produced a negligible effect on Cd^{2+} adsorption by MOS/OCN-1. By calculating the distribution coefficient K_d (mL/g) of MOS/OCN-1 for each cation, it can be found that

Journal Pre-proofs

the K_d^{Cd} value (~10^5 mL/g) in the mixed solution with cation ions of 10 mg/L was 2-3 order of magnitudes higher than K_d^{Zn}, K_d^{Mg}, and K_d^{Ca} (Table S6). Since a material with a K_d value >10^4 mL /g can be considered as an excellent adsorbent with high preference towards the targeted pollutant [26], this result further reflecting the high affinity and selectivity of MOS/OCN-1 for Cd^{2+} over Ca^{2+}, Mg^{2+} and Zn^{2+}.

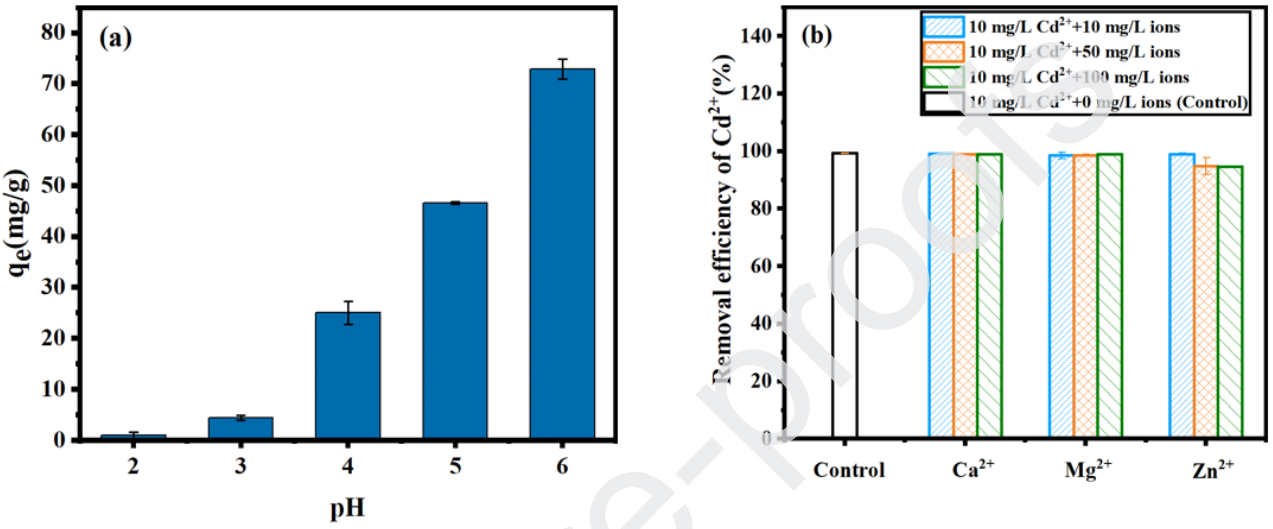

Fig. 4. (a). The effect of pH on Cd^{2+} removal by MOS/OCN-1. Experimental condition: adsorbents dosage= 0.25 g/L, initial Cd^{2+}=20 mg/L, temperature= 25°C. (b) The effect of competing ions, i.e. Ca^{2+}, Mg^{2+} and Zn^{2+} on Cd^{2+} adsorption by MOS/OCN-1. Experimental conditions: adsorbents dosage=0.25 g/L, initial Cd^{2+}=10 mg/L, pH=6.0 ± 0.2, reaction time=24 h, temperature=25°C.

3.4 Mechanisms of Cd^{2+} adsorption on MOS/OCN

3.4.1 The change of structure and composition of MOS/OCN-1

XRD and XPS spectra of MOS/OCN-1 were analyzed before and after Cd^{2+} adsorption in order to elucidate possible adsorption mechanisms. The XRD patterns (Fig. 5a) exhibited several new peaks located at 29.21°, 31.96°, 34.80°, 47.94°, 49.99°, 55.26°, 58.97°, 60.59° and 77.78°after Cd^{2+} adsorption and these peaks can be well assigned as $CdMoO_4$ (JCPDS card No. 07-0209), which indicated a new precipitate $CdMoO_4$ had formed on the surface of MOS/OCN-1. From the results of

Journal Pre-proofs

survey spectra by XPS (Fig. S4 and Table S7), the contents of total O and Mo significantly decreased after adsorption, suggesting that Mo atoms were dissociated from the adsorbents surface, probably in the form of free molybdate ions (ie. MoO_4^{2-}) [22]. Interestingly, the relative content of Mo (IV) decreased from 64.2% to 57.1% after adsorption while Mo (VI) increased from 35.8% to 42.9% (Fig. 5b and Table S7), implying that Mo (IV) was oxidized to Mo (VI) during the adsorption process. Moreover, a new peak located at 163.5eV emerged in the S 2p spectra (Fig. 5c) after adsorption, suggesting the formation of CdS species [20]. However, the characteristic peaks of CdS in the XRD pattern was too weak to be found, which may be ascribed to the low content.

From FTIR analysis (Fig. 5d), the intensity of Mo-OH, located at 881 cm^{-1}[46], decreased significantly after Cd^{2+} adsorption, which suggested that surface oxygen probably dissociated from the adsorbent as MoO_4^{2-}. A redshift in the Mo-O band, from 743 to 766 cm^{-1}, occurred after adsorption, implying that Cd^{2+} interacted with Mo-O-Mo during adsorption [48, 49] and that was in accordance with the production of $CdMoO_4$ (Fig.5a). Because of the low content of CdS, no characteristic peak of Cd-S at around 630 cm^{-1} [50] was found and the peak of Mo-S (500 cm^{-1}) [51] did not change noticeably after Cd^{2+} loading. However, evidence from the XPS spectra suggested that Cd-S interaction also occurred during Cd^{2+} removal. Therefore, combining the results from XRD, XPS and FTIR analyses, it was considered that the formation of $CdMoO_4$ precipitate as well as Cd-S interaction contributed to Cd^{2+} removal by MOS/OCN-1, while the former precipitation showed more obvious evidence.

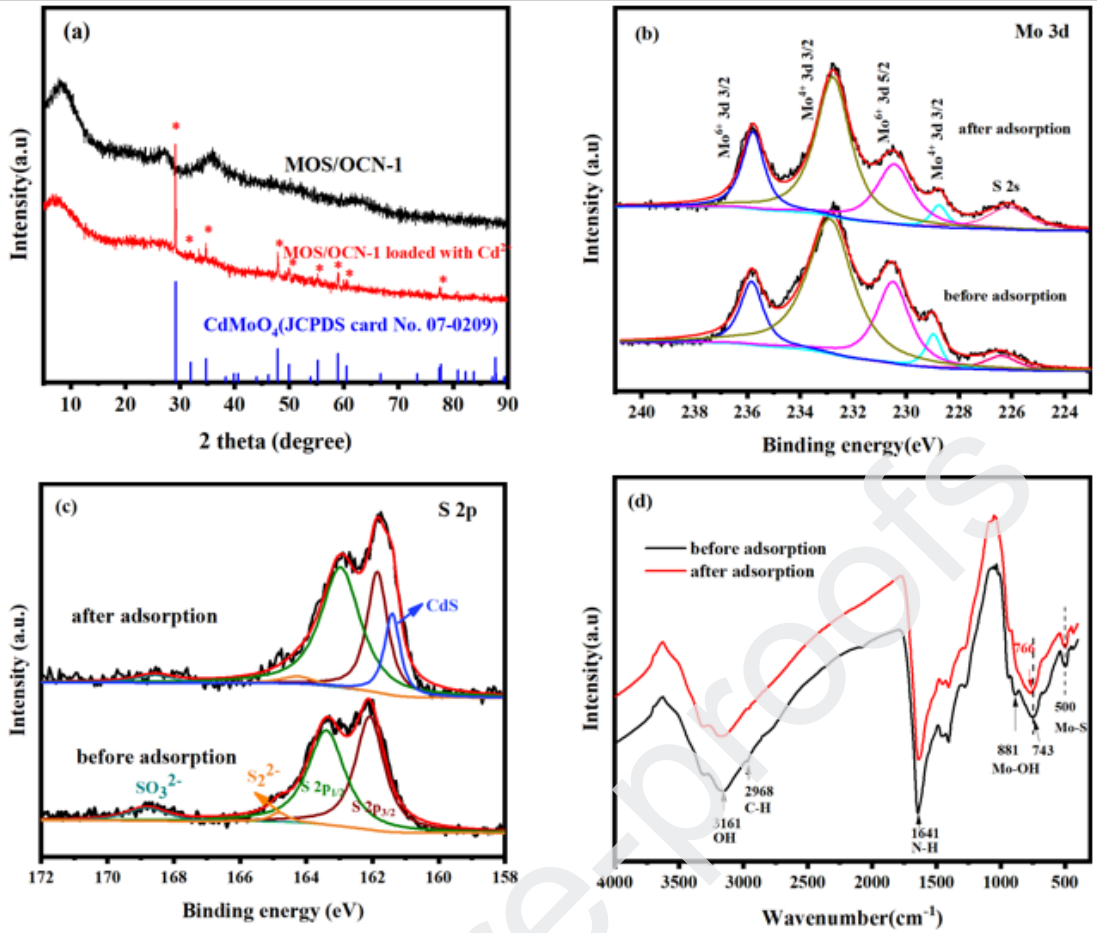

Fig. 5. XRD pattern of MOS/OCN-1 before and after Cd^{2+} adsorption (a). XPS spectra of Mo 3d (b) and S 2p (c) before and after Cd^{2+} adsorption. FTIR spectra of MOS/OCN-1 before and after adsorption (d). Experimental conditions: adsorbents dosage=1 g/L, initial Cd^{2+}=200 mg/L, pH=6.0 ± 0.2, reaction time=24 h, temperature=25°C.

3.4.2 MoO_4^{2-} generation and contribution

In order to identify the production of MoO_4^{2-} and its effect on Cd^{2+} removal, the released MoO_4^{2-} in solution was detected at the end of the adsorption experiment under different pH conditions (Fig. 6). The concentration of MoO_4^{2-} in the control solution (without Cd^{2+} addition) was found to be higher than that in the solution with 20 mg/L Cd^{2+} under all pH conditions (pH 2-6), suggesting that the proportion of free MoO_4^{2-} combined with Cd^{2+} to form precipitate. With pH

Journal Pre-proofs

increasing from 3 to 6, the concentrations of MoO_4^{2-} and total sulphur in solution gradually increased, accompanied by increasing Cd^{2+} adsorption efficiency (Fig. 1b). This result can be explained by two aspects. Due to the coexistence of MoS_2 and MoO_3 in the MOS/OCN-1 (Fig. 1 and 2), the oxidation of MoS_2 (Equation 4) and hydrolysis of MoO_3 (Equation 5) can simultaneously generate MoO_4^{2-} in the solution [22, 52]. The released MoO_4^{2-} could then contribute to Cd^{2+} precipitation by forming $CdMoO_4$ (Equation 6). As the release of H^+ (Equation 4 and 5) would decrease the pH value during Cd^{2+} adsorption (supported by the fact that pH decreased from 6.0 to 4.7 if without any adjustment), therefore, extra OH^- was added into the solution to maintain the targeted pH level of the solution. The addition of OH^- then drove the production of more MoO_4^{2-} for Cd^{2+} removal. Additionally, the corrosion of MoS_2 with the addition of OH^- also produced dissolved sulfur (S^{2-}, HS^- and SO_4^{2-} , etc) and the dissociated S(II) also led to the formation of CdS species (Equation 7), which caused a decrease in dissolved sulphur in Cd^{2+} solution (insert in Fig.6). At pH 2, the concentration of MoO_4^{2-} was little higher than that at pH 3, probably because MoS_2 was partly dissolved in the strongly acidic condition. Further investigation showed that more dissolved MoO_4^{2-} was produced during Cd^{2+} removal by MOS/OCN-1 than MOS-DMF (Fig. S5). Combined with the results of FESEM imaging (Fig.S1), it can be concluded that OCN facilitated active sites exposure on the adsorbent, which further led to better contact of Mo (IV)/Mo (VI) with O_2 and OH^-, thus promoting the production of MoO_4^{2-} and facilitating the precipitation process.

$$2\mathrm{Mo(IV)}S_2 + 3O_2 + 2H_2O \rightarrow 2MoO_4^{2-} + 4S_{dissolved} + 4H^+ \quad (4)$$

$$Mo(VI)O_3 \cdot H_2O \leftrightarrow MoO_4^{2-} + 2H^+ \quad (5)$$

$$MoO_4^{2-} + Cd^{2+} \leftrightarrow CdMoO_4(s) \quad (6)$$

$$S\,(\mathrm{II}) + Cd^{2+} \rightarrow CdS \quad (7)$$

Journal Pre-proofs

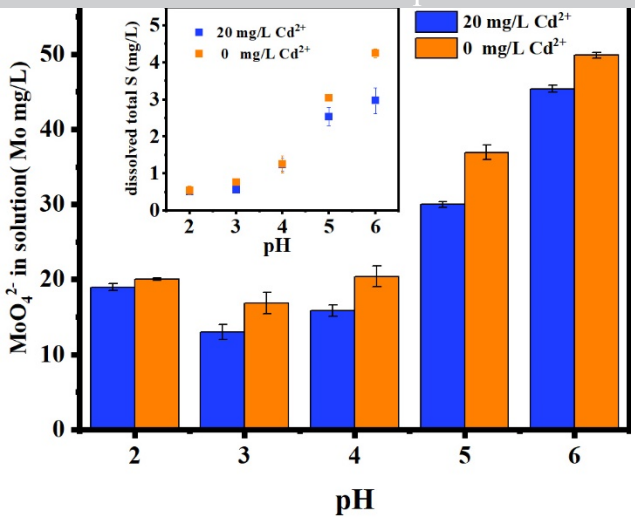

Fig.6. The concentration of MoO_4^{2-} and dissolved total S after Cd^{2+} adsorption by MOS/OCN-1 under different pH conditions. Experimental conditions: adsorbents dosage=0.25 g/L, initial Cd^{2+}=20 mg/L, reaction time=24 h, temperature=25°C.

3.4.3 The role of Mo (IV) and Mo (VI) on Cd^{2+} removal

To further evaluate the contributions of MoS_2 oxidation (Equation 4) and MoO_3 hydroxylation (Equation 5) to Cd^{2+} removal, a MoO_3/OCN hybrid composite was prepared (Fig.S6) and the adsorption performance was compared to that of MOS/OCN-1. In Fig.7a, it may be observed that MoO_3/OCN exhibited a worse adsorption performance than MOS/OCN-1 with a capacity of only 20 mg/g, even though there were more Mo(VI) present in MoO_3/OCN (Fig.S7). A similar poor adsorption efficiency from pure MoO_3 has also been reported in a previous study [23]. It should be noted that the dissolved MoO_4^{2-} from MoO_3/OCN was significantly lower than that from MOS/OCN-1 in both pure water and in Cd^{2+} solution (Fig. 7b), which indicated that production of MoO_4^{2-} from MoO_3 hydrolyzation still limited in acidic condition, due to the relatively low hydrolysis constant value of MoO_3 ($Ka=10^{-11.923}$~$10^{-18.84}$) [53]. However, for MOS/OCN-1, besides intrinsic MoO_3 hydrolyzation, Mo(IV) oxidation in hybrid composite might also contribute greatly to produce more

Journal Pre-proofs

416 MoO_4^{2-}. MoO_4^{2-} produced during the treatment by MOS/OCN-1 caused rapid precipitation of Cd^{2+}

417 on the surface of OCN, thus giving rise to better removal efficiency.

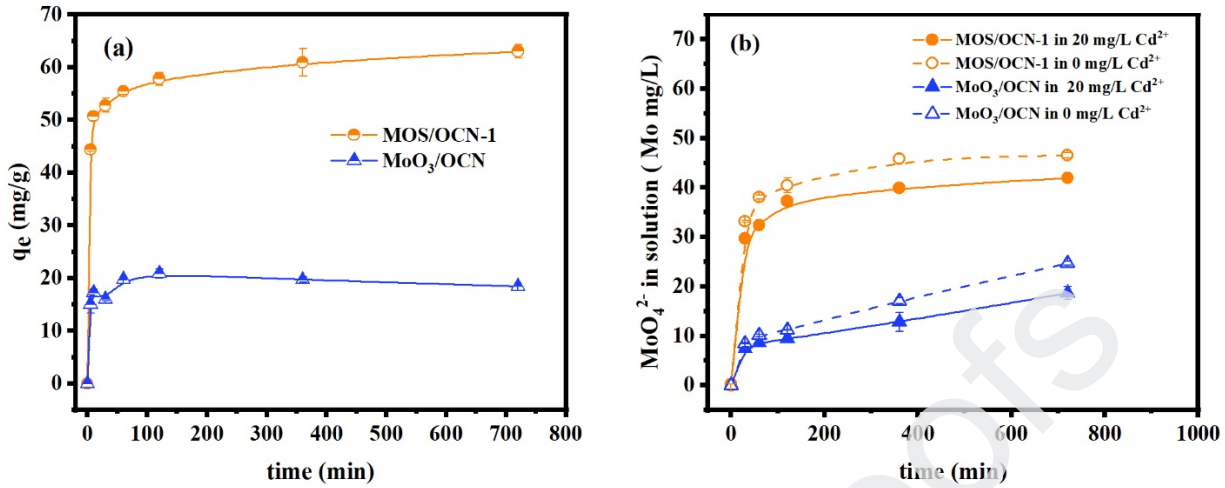

418

419 **Fig.7**. (a) Cd^{2+} adsorption performance by MOS/OCN-1 and MoO_3/OCN. (b) Free molybdate ions in Cd^{2+}

420 solution and pure water treated by MOS/OCN-1 and MoO_3/OCN. Experimental conditions: adsorbents

421 dosage = 0.25 g/L, initial Cd^{2+}=20 mg/L, pH=6.0 ± 0.2, reaction time=12 h, temperature=25°C.

422 It should be noted that the adsorption efficiency of MOS/OCN-1 decreased from 99.2% to 65.3%

423 after three times recycling (Fig. S8), which may due to the loss of Mo, S active species (Fig. 6).

424 Meanwhile, the chemical structures of MOS/OCN-1 may also be altered after several sorption-

425 desorption cycles, because the desorption process involved the use of acid substance HNO_3, which

426 could react with $CdMoO_4$ and CdS found on the surface of the adsorbent [54, 55]. Nevertheless,

427 considering the high-efficiency and relatively low-cost of MOS/OCN, MOS/OCN-1 might still showed

428 a potential in *in-situ* Cd^{2+} remediation.

429 Above all, the adsorption process of Cd^{2+} on hybrid adsorbents can be summarised as follows.

430 The oxidation of MoS_2 and the hydrolyzation of MoO_3 on OCN played a significant role for Cd^{2+}

431 removal by producing MoO_4^{2-}, which in turn precipitated Cd^{2+}. In the meantime, the dissolved S (II)

432 from the oxidized MoS_2 also interacted with Cd^{2+} by forming CdS species. Herein, OCN functioned

Journal Pre-proofs

as a stable interface with large surface area to expose more active species/sites (Mo (IV)， Mo(VI) and S (II)) to interact with Cd^{2+}, which finally induced the enhancement of Cd^{2+} removal.

4. Conclusions

In this work, Mo and S were simultaneously introduced on oxygen-doped carbon nitride (OCN) through a facile one-step solvothermal process. The hybrid composite MOS/OCN-1 achieved enhanced performance for Cd^{2+} removal with a maximum adsorption capacity of 293.8 mg/g, 8.7 times higher than that of OCN alone and superior to many other carbon-based materials. Cd^{2+} adsorption followed a pseudo-second order model and the fitting to an intraparticle diffusion model indicated that chemical interaction and particle diffusion process controlled the adsorption rate. Moreover, good anti-interference ability towards Cd^{2+} under the presence of different coexisting ions like Ca^{2+}, Mg^{2+}, Zn^{2+} was also achieved by MOS/OCN-1. OCN provided a large surface area and functioned as an interface to inhibit the agglomeration of MoS_2 and MoO_3 nanoparticles, which acted to expose more active sites for Cd^{2+} effective adsorption. Besides the well-known soft-soft Cd-S interaction, the production of $CdMoO_4$ also contributed greatly to Cd^{2+} removal, where the release of MoO_4^{2-} was controlled both by the dissociation of intrinsic Mo(VI) and oxidization of Mo(IV). This work has highlighted a potential, effective and low-cost adsorbent suitable for *in-situ* Cd^{2+} remediation, and has suggested related mechanisms, especially the effect of Mo atoms on the adsorption process. Further studies on the general treatment capabilities of MOS/OCN for other heavy metals, or those capabilities of other layered-structure materials with Mo and S modifications, will be conducted in the future.

Acknowledgements

This work was supported by the National Key R&D Program of China (2017YFA0207204), the National Natural Science Foundation of China (Grant No. 21806175) and Medical Technologies and Advanced Materials Strategic Theme at Nottingham Trent University. We thank Dr Mick Cooper for proof reading.

References

[1] Q. Zhou, B. Liao, L. Lin, W. Qiu, Z. Song, Adsorption of Cu(II) and Cd(II) from aqueous solutions by ferromanganese binary oxide-biochar composites, Sci Total Environ, 615 (2018) 115-122.

[2] L. Liu, Q. Peng, G. Qiu, J. Zhu, W. Tan, C. Liu, L. Zheng, Z. Dang, Cd^{2+} adsorption performance of tunnel-structured manganese oxides driven by electrochemically controlled redox, Environmental pollution, 244 (2019) 783-791.

[3] C. Zhang, Z. Yu, G. Zeng, B. Huang, H. Dong, J. Huang, Z. Yang, J. Wei, L. Hu, Q. Zhang, Phase transformation of crystalline iron oxides and their adsorption abilities for Pb and Cd, Chemical Engineering Journal, 284 (2016) 247-259.

[4] T. Priya, N. Dhanalakshmi, S. Thennarasu, N. Thinakaran, A novel voltammetric sensor for the simultaneous detection of Cd^{2+} and Pb^{2+} using graphene oxide/kappa-carrageenan/l-cysteine nanocomposite, Carbohydr Polym, 182 (2018) 199-206.

[5] W.W. Tang, G.M. Zeng, J.L. Gong, J. Liang, P. Xu, C. Zhang, B.B. Huang, Impact of humic/fulvic acid on the removal of heavy metals from aqueous solutions using nanomaterials: a review, Sci Total Environ, 468-469 (2014) 1014-1027.

[6] X. Cai, J. He, L. Chen, K. Chen, Y. Li, K. Zhang, Z. Jin, J. Liu, C. Wang, X. Wang, L. Kong, J. Liu, A 2D-g-C_3N_4 nanosheet as an eco-friendly adsorbent for various environmental pollutants in water, Chemosphere, 171 (2017) 192-201.

[7] J.H. Park, Y.S. Ok, S.H. Kim, J.S. Cho, J.S. Heo, R.D. Delaune, D.C. Seo, Competitive adsorption of heavy metals onto sesame straw biochar in aqueous solutions, Chemosphere, 142 (2016) 77-83.

[8] C. Liu, S. Dong, Y. Chen, Enhancement of visible-light-driven photocatalytic activity of carbon plane/g-C_3N_4/TiO_2 nanocomposite by improving heterojunction contact, Chemical Engineering Journal, 371 (2019) 706-718.

[9] C. Shen, C. Chen, T. Wen, Z. Zhao, X. Wang, A. Xu, Superior adsorption capacity of g-C_3N_4 for heavy metal ions from aqueous solutions, J Colloid Interface Sci, 456 (2015) 7-14.

[10] R. Kumar, M.A. Barakat, F.A. Alseroury, Oxidized g-C_3N_4/polyaniline nanofiber composite for the selective removal of hexavalent chromium, Scientific reports, 7 (2017) 12850.

[11] D. Peng, W. Jiang, F.-F. Li, L. Zhang, R.-P. Liang, J.-D. Qiu, One-Pot Synthesis of Boron Carbon Nitride Nanosheets for Facile and Efficient Heavy Metal Ions Removal, ACS Sustainable Chemistry & Engineering, 6 (2018) 11685-11694.

[12] X.W. Yidong Zou, Yuejie Ai, Yunhai Liu, Yongfei Ji, Hongqing Wang, Tasawar Hayat, Ahmed Alsaedi, Wenping Hu and Xiangke Wang, β-Cyclodextrin modified graphitic carbon nitride for the removal of pollutants from aqueous solution: experimental and theoretical calculation study, Journal of Materials Chemistry A, 4 (2016) 14170-14179.

[13] P. Wang, L. Yin, J. Wang, C. Xu, Y. Liang, W. Yao, X. Wang, S. Yu, J. Chen, Y. Sun, X. Wang, Superior immobilization of U(VI) and 243 Am(III) on polyethyleneimine modified lamellar carbon nitride composite from water environment, Chemical Engineering Journal, 326 (2017) 863-874.

[14] P. Qiu, C. Xu, H. Chen, F. Jiang, X. Wang, R. Lu, X. Zhang, One step synthesis of oxygen doped porous graphitic carbon nitride with remarkable improvement of photo-oxidation activity: Role of oxygen on visible light photocatalytic activity, Applied Catalysis B: Environmental, 206 (2017) 319-327.

[15] L. Wang, Y. Shi, D. Yao, H. Pan, H. Hou, J. Chen, J.C. Crittenden, Cd complexation with mercapto-functionalized attapulgite (MATP): Adsorption and DFT study, Chemical Engineering Journal, 366 (2019) 569-576.

Journal Pre-proofs
[16] J. Ali, H. Wang, J. Iqbal, A. Khan, T. Wang, R. Zhao, A. Shahzad, Z. Chen, Z. Chen, Efficient, stable and selective adsorption of heavy metals by thio-functionalized layered double hydroxide in diverse types of water, Chemical Engineering Journal, 332 (2018) 387-397.
[17] K. Ai, C. Ruan, M. Shen, L. Lu, MoS_2 Nanosheets with Widened Interlayer Spacing for High-Efficiency Removal of Mercury in Aquatic Systems, Advanced Functional Materials, 26 (2016) 5542-5549.
[18] F. Jia, Q. Wang, J. Wu, Y. Li, S. Song, Two-Dimensional Molybdenum Disulfide as a Superb Adsorbent for Removing Hg^{2+} from Water, ACS Sustainable Chemistry & Engineering, 5 (2017) 7410-7419.
[19] M. Zhang, F. Jia, M. Dai, S. Song, Combined electrosorption and chemisorption of low concentration Pb(II) from aqueous solutions with molybdenum disulfide as electrode, Applied Surface Science, 455 (2018) 258-266.
[20] Q. Wang, L. Yang, F. Jia, Y. Li, S. Song, Removal of Cd (II) from water by using nano-scale molybdenum disulphide sheets as adsorbents, Journal of Molecular Liquids, (2018).
[21] F. Jia, X. Zhang, S. Song, AFM study on the adsorption of Hg^{2+} on natural molybdenum disulfide in aqueous solutions, Phys Chem Chem Phys, 19 (2017) 3837-3844.
[22] X. Zhang, F. Jia, B. Yang, S. Song, Oxidation of Molybdenum Disulfide Sheet in Water under in Situ Atomic Force Microscopy Observation, The Journal of Physical Chemistry C, 121 (2017) 9938-9943.
[23] Y. Wu, X. Cheng, X. Zhang, Y. Xu, S. Gao, H. Zhao, L. Huo, High efficient and selective removal of Pb^{2+} through formation of lead molybdate on alpha-MoO_3 porous nanosheets array, J Colloid Interface Sci, 491 (2017) 80-88.
[24] F. Jia, C. Liu, B. Yang, X. Zhang, H. Yi, J. Ni, S. Song, Thermal Modification of the Molybdenum Disulfide Surface for Tremendous Improvement of Hg^{2+} Adsorption from Aqueous Solution, ACS Sustainable Chemistry & Engineering, 6 (2018) 9065-9073.
[25] H. Liu, X. Chen, L. Deng, M. Ding, J. Li, X. He, Perpendicular growth of few-layered MoS_2 nanosheets on MoO_3 nanowires fabricated by direct anion exchange reactions for high-performance lithium-ion batteries, Journal of Materials Chemistry A, 4 (2016) 17764-17772.
[26] M.L. Feng, D. Sarma, X.H. Qi, K.Z. Du, X.Y. Huang, M.G. Kanatzidis, Efficient Removal and Recovery of Uranium by a Layered Organic-Inorganic Hybrid Thiostannate, J Am Chem Soc, 138 (2016) 12578-12585.
[27] J. Xie, J. Zhang, S. Li, F. Grote, X. Zhang, H. Zhang, R. Wang, Y. Lei, B. Pan, Y. Xie, Controllable disorder engineering in oxygen-incorporated MoS_2 ultrathin nanosheets for efficient hydrogen evolution, J Am Chem Soc, 135 (2013) 17881-17888.
[28] M.-h. Wu, L. Li, Y.-c. Xue, G. Xu, L. Tang, N. Liu, W.-y. Huang, Fabrication of ternary GO/g- C_3N_4 /MoS_2 flower-like heterojunctions with enhanced photocatalytic activity for water remediation, Applied Catalysis B: Environmental, 228 (2018) 103-112.
[29] S. Kizito, H. Luo, S. Wu, Z. Ajmal, T. Lv, R. Dong, Phosphate recovery from liquid fraction of anaerobic digestate using four slow pyrolyzed biochars: Dynamics of adsorption, desorption and regeneration, Journal of Environmental Management, 201 (2017) 260-267.
[30] A. Zhu, L. Qiao, P. Tan, W. Zeng, Y. Ma, R. Dong, J. Pan, Boosted electrocatalytic activity of nitrogen-doped porous carbon triggered by oxygen functional groups, J Colloid Interface Sci, 541 (2019) 133-142.
[31] Y.-J. Song, J.-T. Ren, G. Yuan, Y. Yao, X. Liu, Z.-Y. Yuan, Facile synthesis of Mo_2C nanoparticles on N-doped carbon nanotubes with enhanced electrocatalytic activity for hydrogen evolution and oxygen reduction reactions, Journal of Energy Chemistry, 38 (2019) 68-77.
[32] Q. Gu, H. Sun, Z. Xie, Z. Gao, C. Xue, MoS2-coated microspheres of self-sensitized carbon nitride for efficient photocatalytic hydrogen generation under visible light irradiation, Applied Surface Science, 396 (2017) 1808-1815.
[33] M. Wu, J. Zhan, K. Wu, Z. Li, L. Wang, B. Geng, L. Wang, D. Pan, Metallic 1T MoS_2 nanosheet arrays vertically grown on activated carbon fiber cloth for enhanced Li-ion storage performance, J. Mater. Chem. A, 5 (2017) 14061-14069.
[34] W.-H. Hu, X. Shang, J. Xue, B. Dong, J.-Q. Chi, G.-Q. Han, Y.-R. Liu, X. Li, K.-L. Yan, Y.-M. Chai, C.-G. Liu, Activating MoS_2/CNs by tuning (001) plane as efficient electrocatalysts for hydrogen evolution reaction, International Journal of

Journal Pre-proofs
Hydrogen Energy), 42 (2017) 2088-2099.
[35] L. Ma, Q. Wang, S.M. Islam, Y. Liu, S. Ma, M.G. Kanatzidis, Highly Selective and Efficient Removal of Heavy Metals by Layered Double Hydroxide Intercalated with the MoS_4^{2-} Ion, J Am Chem Soc, 138 (2016) 2858-2866.
[36] T. Liu, S. Zheng, L. Yang, Magnetic zirconium-based metal-organic frameworks for selective phosphate adsorption from water, J Colloid Interface Sci, 552 (2019) 134-141.
[37] G.G. Haciosmanoglu, T. Dogruel, S. Genc, E.T. Oner, Z.S. Can, Adsorptive removal of bisphenol A from aqueous solutions using phosphonated levan, Journal of hazardous materials, 374 (2019) 43-49.
[38] G. Tan, Z. Li, H. Yuan, D. Xiao, Sorption of Cadmium from Aqueous Solution with a Highly Effective Sorbent – B-Doped g-C_3N_4, Separation Science and Technology, 49 (2014) 1566-1573.
[39] S. Guo, C. Zhang, F. Zhang, X. Li, P. Zhang, L. Luo, Synthesis of magnetic g-C_3N_4 by one-step method and its adsorption performance for Cd(II), IOP Conference Series: Materials Science and Engineering, 274 (2017) 012091.
[40] D. Ko, J.S. Lee, H.A. Patel, M.H. Jakobsen, Y. Hwang, C.T. Yavuz, H.C.B. Hansen, H.R. Andersen, Selective removal of heavy metal ions by disulfide linked polymer networks, Journal of hazardous materials, 332 (2017) 140-148.
[41] Q. Tao, Y. Chen, J. Zhao, B. Li, Y. Li, S. Tao, M. Li, Q. Li, Q. Xu, Y. Li, H. Li, B. Li, Y. Chen, C. Wang, Enhanced Cd removal from aqueous solution by biologically modified biochar derived from digestion residue of corn straw silage, Sci Total Environ, 674 (2019) 213-222.
[42] K. Brahmi, W. Bouguerra, K. Missaoui, Z. Tlili, E. Elaloui, M. Loungou, B. Hamrouni, Highly cost-effective and reuse-oriented treatment of cadmium-polluted mining wastewater by electrocoagulation process, Journal of Environmental Engineering, 142 (2016) 04016061.
[43] C. Zhou, J. Ni, D. Zhang, C. Sun, Cellulosic adsorbent functionalized with macrocyclic pyridone pentamer for selectively removing metal cations from aqueous solutions, Carbohydrate Polymers, 217 (2019) 1-5.
[44] Z. Wu, W. Deng, W. Zhou, J. Luo, Novel magnetic polysaccharide/graphene oxide @Fe_3O_4 gel beads for adsorbing heavy metal ions, Carbohydr Polym, 216 (2019) 119-128.
[45] J. Liu, X. Ge, X. Ye, G. Wang, H. Zhang, H. Zhou, Y. Zhang, H. Zhao, 3D graphene/δ-MnO_2 aerogels for highly efficient and reversible removal of heavy metal ions, Journal of Materials Chemistry A, 4 (2016) 1970-1979.
[46] J. Wang, W. Zhang, X. Yue, Q. Yang, F. Liu, Y. Wang, D. Zhang, Z. Li, J. Wang, One-pot synthesis of multifunctional magnetic ferrite–MoS_2–carbon dot nanohybrid adsorbent for efficient Pb(II) removal, Journal of Materials Chemistry A, 4 (2016) 3893-3900.
[47] Y. Gao, X. Ren, J. Wu, T. Hayat, A. Alsaedi, C. Cheng, C. Chen, Graphene oxide interactions with co-existing heavy metal cations: adsorption, colloidal properties and joint toxicity, Environmental Science: Nano, 5 (2018) 362-371.
[48] L. Kong, Z. Li, X. Huang, S. Huang, H. Sun, M. Liu, L. Li, Efficient removal of Pb(II) from water using magnetic Fe_3S_4/reduced graphene oxide composites, Journal of Materials Chemistry A, 5 (2017) 19333-19342.
[49] S. Mostafa Hosseinpour-Mashkani, M. Maddahfar, A. Sobhani-Nasab, Novel silver-doped $CdMoO_4$: synthesis, characterization, and its photocatalytic performance for methyl orange degradation through the sonochemical method, Journal of Materials Science: Materials in Electronics, 27 (2015) 474-480.
[50] L. Zhang, X. Li, Z. Mu, J. Miao, K. Wang, R. Zhang, S. Chen, A novel composite of CdS nanorods growing on a polyaniline-Cd^{2+} particles surface with excellent formaldehyde gas sensing properties at low temperature, RSC Advances, 8 (2018) 30747-30754.
[51] G. Angamuthu, D.B. Babu, K. Ramesha, V. Rangarajan, MoS_2 anchored carbon nitride based mesoporous material as a polysulfide barrier for high capacity lithium-sulfur battery, Journal of Electroanalytical Chemistry, 843 (2019) 37-46.
[52] B. Mondal, A. Mahendranath, A. Som, S. Bose, T. Ahuja, A.A. Kumar, J. Ghosh, T. Pradeep, Rapid reaction of MoS_2 nanosheets with Pb^{2+} and Pb^{4+} ions in solution, Nanoscale, 10 (2018) 1807-1814.
[53] T.P. Dadze, G.A. Kashirtseva, M.P. Novikov, A.V. Plyasunov, Solubility of calcium molybdate in aqueous solutions at 573 K and thermodynamics of monomer hydrolysis of Mo(VI) at elevated temperatures, Monatshefte für Chemie - Chemical Monthly, 149 (2017) 261-282.

Journal Pre-proofs

[54] L. Fang, L. Li, Z. Qu, H. Xu, J. Xu, N. Yan, A novel method for the sequential removal and separation of multiple heavy metals from wastewater, Journal of hazardous materials, 342 (2018) 617-624.

[55] W.-S. Wang, L. Zhen, C.-Y. Xu, W.-Z. Shao, Z.-L. Chen, Formation of $CdMoO_4$ porous hollow nanospheres via a self-assembly accompanied with Ostwald ripening process and their photocatalytic performance, CrystEngComm, 15 (2013).

Journal Pre-proofs

589 **Figure captions**

590 **Fig. 1**. (a) XRD patterns of synthesized adsorbents of MOS/OCN-x, MOS-DMF, and OCN; (b) Cd^{2+} adsorption
591 capacities of MOS/OCN-x, MOS-DMF and OCN. Experimental conditions: adsorbents dosage=0.25 g/L, initial
592 Cd^{2+}= 20 mg/L, pH=6.0, reaction time=24 h, temperature=25°C.

593 **Fig.2.** XPS spectra of MOS/OCN-1: Mo 3d (a), S 2p (b) and O 1s (c). MOS-DMF: Mo 3d (d), S 2p (e) and O 1s
594 (f).

595 **Fig. 3**. Cd^{2+} adsorption kinetics fitted with the pseudo-second order model (a) and intraparticle diffusion
596 model (b). Experimental condition: adsorbents dosage= 0.25 g/L, initial Cd^{2+}=20 mg/L, pH=6.0 ± 0.2,
597 temperature=25°C. Cd^{2+} adsorption isotherm curve fitted with Langmuir, Freundlich and Sips model (c).
598 Experimental conditions: adsorbents dosage=0.25 g/L, initial Cd^{2+}=15-600 mg/L, pH=6.0 ± 0.2, reaction
599 time=24h, temperature=25°C.

600 **Fig. 4**. (a). The effect of pH on Cd^{2+} removal by MOS/OCN-1. Experimental condition: adsorbents dosage=
601 0.25 g/L, initial Cd^{2+}=20 mg/L, temperature= 25°C. (b) The effect of competing ions, i.e. Ca^{2+}, Mg^{2+} and Zn^{2+}
602 on Cd^{2+} adsorption by MOS/OCN-1. Experimental conditions: adsorbents dosage=0.25 g/L, initial Cd^{2+}=10
603 mg/L, pH=6.0 ± 0.2, reaction time=24 h, temperature=25°C.

604 **Fig. 5**. XRD pattern of MOS/OCN-1 before and after Cd^{2+} adsorption (a). XPS spectra of Mo 3d (b) and S 2p (c)
605 before and after Cd^{2+} adsorption. FTIR spectra of MOS/OCN-1 before and after adsorption (d). Experimental
606 conditions: adsorbents dosage=1 g/L, initial Cd^{2+}=200 mg/L, pH=6.0 ± 0.2, reaction time=24 h,
607 temperature=25°C

608 **Fig.6.** The concentration of MoO_4^{2-} and dissolved total S after Cd^{2+} adsorption by MOS/OCN-1 under different
609 pH conditions. Experimental conditions: adsorbents dosage=0.25 g/L, initial Cd^{2+}=20 mg/L, reaction time=24

Journal Pre-proofs

Journal Pre-proofs

610 h, temperature=25°C.

611 **Fig.7**. (a) Cd^{2+} adsorption performance by MOS/OCN-1 and MoO_3/OCN. (b) Free molybdate ions in Cd^{2+}

612 solution and pure water treated by MOS/OCN-1 and MoO_3/OCN. Experimental conditions: adsorbents

613 dosage = 0.25 g/L, initial Cd^{2+}=20 mg/L, pH=6.0 ± 0.2, reaction time=12 h, temperature=25°C

614

615

Journal Pre-proofs

Journal Pre-proofs

Tables

Table 1

Comparison of maximum Cd^{2+} adsorption capacities by different adsorbents.

Adsorbent	q_m (mg/g)	Reference
g-C_3N_4	112.4	[9]
2D –g-C_3N_4	94.4	[6]
B-doped g-C_3N_4	159.2	[38]
Fe_3O_4-g-C_3N_4	204.5	[39]
Disulfide linked polymer networks (COP 63)	9.9	[40]
TCB-700 (biologically modified biochar)	175.4	[41]
OCN	33.9	This work
MOS-DMF	139.4	This work
MOS/OCN-1	293.8	This work

Journal Pre-proofs